Coexistence of tonic firing and bursting in cortical neurons

Flavio Fröhlich[1,2] and Maxim Bazhenov[1]

[1]*Salk Institute, 10010 North Torrey Pines Rd., La Jolla, California 92037, USA*
[2]*Division of Biology, University of California, San Diego, La Jolla, California 92093, USA*

Sustained neuronal activity can be broadly classified as either tonic firing or bursting. These two major patterns of neuronal oscillations are state dependent and may coexist. The dynamics and intracellular mechanisms of transitions between tonic firing and bursting in cortical networks remain poorly understood. Here we describe a detailed two-compartment conductance-based cortical neuron model which exhibits bistability with hysteresis between tonic firing and bursting for elevated extracellular potassium concentration. The study explains the ionic and dynamical mechanisms of burst generation and reveals the conditions underlying coexistence of two different oscillatory modes as a function of neuronal excitability.

PACS number(s): 87.18.Sn

I. INTRODUCTION

Oscillatory activity is an emerging property of many biological systems. In the brain, neuronal oscillations modulate cortical excitability and are critically involved in almost every cognitive task including information coding, memory formation, and perception [1]. Neuronal oscillations result from the activity of individual neurons that can be broadly classified as tonic spiking (unimodal distribution of interspike intervals) and bursting (multimodal distribution with distinct peaks for intraburst intervals). Many neuron classes display transitions between tonic spiking and bursting as a function of the brain state (e.g., sleep versus wakefulness) [2]; these transitions can modify the transfer mode of a neuronal population. Understanding the dynamical mechanisms underlying the existence of tonic spiking and bursting oscillations and conditions that trigger transitions between these patterns of neuronal activity is critical for understanding processing of sensory information in the brain.

An increase in intrinsic excitability can cause bursting in cells which usually fire single action potentials. Extracellular potassium concentration ($[K^+]_o$) has been shown to modulate intrinsic excitability [3]. It is well established that $[K^+]_o$ increases during epileptogenesis [4] and may be critically involved in synchronized burst oscillations during several seizure types [5]. Little, however, is known about the underlying dynamics of these state-dependent transitions between different oscillatory modes. Here, we show that nonsynaptic, spontaneous activity in hippocampal region CA3 *in vitro* switches from single spikes to bursting when $[K^+]_o$ is increased. We then build a conductance-based model of a cortical neuron which we show to exhibit bistability with hysteresis between tonic firing and bursting for elevated $[K^+]_o$. Using fast-slow analysis, we explain the mechanism of bursting and reveal the source of bistability in this system for a range of $[K^+]_o$.

II. CONDUCTANCE-BASED MODEL

The conductance-based model used in our study includes a dendritic and an axo-somatic compartment reflecting the functional morphology of cortical neurons [6]. Motivation for the choice of a two-compartmental model is that different firing patterns (e.g., different levels of spike frequency adaptation for regular spiking neuron versus fast spiking interneuron) can be easily modeled by varying the electrical coupling between the two compartments [6]. Here, we model a pyramidal cell with spike frequency adaptation for injection of a depolarizing step current,

$$C_m dV_D/dt = - g_L(V_D - E_L) - g_{KL,D}(V_D - E_K)$$
$$- g(V_D - V_S)/S_D - I_D^{ionic}$$

$$g(V_S - V_D)/S_S = - g_{KL,S}(V_S - E_K) - I_S^{ionic}, \qquad (1)$$

where V_D and V_S are dendritic and somatic membrane voltages, respectively, $g=0.1$ mS is the coupling conductance between the two compartments, I_D^{ionic} and I_S^{ionic} are the ionic currents in the two compartments, $C_m=0.75~\mu F/cm^2$ is the membrane capacitance, and $g_L=0.03$ mS/cm^2, $g_{KL,D}=0.01$ mS/cm^2, $g_{KL,S}=0.1$ mS/cm^2, E_L, and E_K are the conductances and equilibrium potentials of the mixed and potassium-mediated dendritic and somatic leak currents, respectively. The surface areas of the dendritic and somatic compartments are $S_D=1.65\times10^{-4}$ cm^2 and $S_S=10^{-6}$ cm^2, respectively. All ionic currents are of the form $I_j=g_j(V_{D,S}-E_j)$ with conductance g_j and equilibrium potential E_j. The conductance g_j is written as

$$g_j = G_j m^M h^H, \qquad (2)$$

with maximal conductance G_j and voltage-dependent activation and inactivation variables m and h. The activation and inactivation dynamics are described by first-order kinetics of the form $\tau\dot{x}=-(x-x_\infty)$ where $x \in \{m,h\}$. Specifically, the dendritic compartment is endowed with voltage-gated transient and persistent sodium ($I_{Na,D}$ and $I_{Nap,D}$), slow voltage-dependent and calcium-dependent noninactivating potassium (I_{Km} and I_{KCa}), high-threshold calcium I_{Ca}, and hyperpolarization-activated depolarizing I_h currents [7]:

$$I_D^{ionic} = I_{Na,D} + I_{Nap,D} + I_{Km} + I_{KCa} + I_{Ca} + I_h. \qquad (3)$$

The axo-somatic compartment exhibits a transient and persistent sodium current ($I_{Na,S}$ and $I_{Nap,S}$) and a delayed-rectifier potassium I_{Kv} current [8]:

$$I_S^{ionic} = I_{Na,S} + I_{Nap,S} + I_{Kv}. \tag{4}$$

The maximal conductances are $G_{Na,D} = 1$, $G_{Nap,D} = 3.5$, $G_{Km} = 0.01$, $G_{KCa} = 2.5$, $G_{Ca} = 0.015$, $G_h = 0.05$, $G_{Na,S} = 3000$, $G_{Nap,S} = 0\text{-}3.5$, and $G_{Kv} = 200$ (all conductances in mS/cm^2, voltage-dependent conductances scaled with temperature adjustment factor $\alpha = 2.95$ [6]). The equilibrium potentials were $E_{Na} = 50$ mV and $E_{Ca} = 140$ mV. The equilibrium potential E_K for potassium conductances is determined by the Nernst equation. The voltage-independent leak conductance g_L, with equilibrium potential E_L given by the Goldman-Hodgkin-Katz equation, defines the resting potential [9,10]:

$$E_K = 26.64 \ln \frac{[K^+]_o}{[K^+]_i}$$

$$E_L = 26.64 \ln \frac{[K^+]_o + 0.085[Na^+]_o + 0.1[Cl^-]_i}{[K^+]_i + 0.085[Na^+]_i + 0.1[Cl^-]_o}, \tag{5}$$

where the ion concentrations are set to $[Na^+]_o = 130$ mM, $[Na^+]_i = 20$ mM, $[Cl^-]_o = 130$ mM, $[Cl^-]_i = 8$ mM. Intracellular calcium dynamics are described by

$$d[Ca^{2+}]_i/dt = -5.18 \times 10^{-5} I_{Ca} + ([Ca^{2+}]_{i(eq)} - [Ca^{2+}]_i)/\tau_{Ca}, \tag{6}$$

where $[Ca^{2+}]_{i(eq)} = 240$ nM is the equilibrium concentration and $\tau_{Ca} = 300$ ms is the time constant for intracellular Ca^{2+} removal. All bifurcation diagrams are built using XPP-AUTO [11].

III. RESULTS

Potassium-mediated currents contribute to the resting state of the membrane voltage and act against any depolarizing ion currents. Therefore, an increase in $[K^+]_o$, which weakens potassium currents, causes an increase in intrinsic excitability. Here, we show how a change in $[K^+]_o$ modulates the spontaneous activity patterns mediated by intrinsic conductances in the absence of any current injection; we recorded nonsynaptic, spontaneous activity in hippocampal region CA3 *in vitro* for $[K^+]_o = 2.5$ mM and $[K^+]_o = 6.5$ mM (extracellular single unit recordings [12]). For low $[K^+]_o$, all units which we recorded from fired single action potentials most of the time. Increasing $[K^+]_o$ caused bursting to become the prevalent firing pattern (representative units in Fig. 1). Bottom panel of Fig. 1 displays the probability distribution of instantaneous frequencies (inverse of interspike intervals) for two cells and two $[K^+]_o$ concentrations. It shows that the cells recorded in high potassium ($[K^+]_o = 6.5$ mM) clearly exhibit bimodal distribution of instantaneous frequencies with one peak corresponding to frequencies higher than 130 Hz (interspike intervals < 7.7 ms) and another one corresponding to frequencies less than 4.8 Hz (interspike intervals > 208 ms). Only the latter peak corresponding to interspike intervals larger than 208 ms was found for neurons recorded in low potassium ($[K^+]_o = 2.5$ mM).

To explain these data and to understand the dynamical mechanisms of the transition between different oscillatory
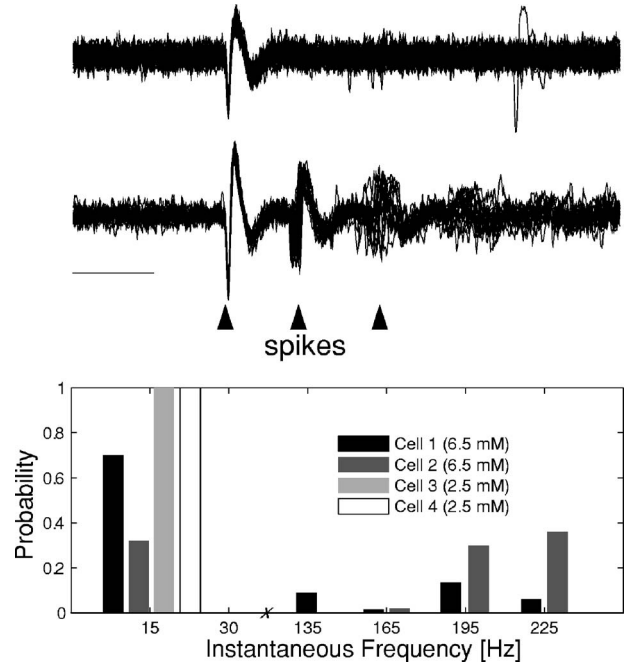
FIG. 1. Top panels: Representative single unit activity for $[K^+]_o = 2.5$ mM (top) and $[K^+]_o = 6.5$ mM (bottom) in hippocampal region CA3. Ten traces are aligned by the first spike in a sequence. In high $[K^+]_o$ solution, the neurons fired bursts with several spikes. Scale bar: 5 ms. Bottom panel: Probability distribution of instantaneous frequencies (calculated as inverse of interspike intervals, $N = 204$) for two cells for each $[K^+]_o$ concentration. Cells 1 and 2 ($[K^+]_o = 6.5$ mM) exhibit nonzero probabilities for instantaneous frequencies higher than 130 Hz, corresponding to spiking during bursts. Cells 3 and 4 ($[K^+]_o = 2.5$ mM) never show instantaneous frequencies exceeding 4.8 Hz (that corresponds to interspike intervals > 208 ms).

modes, we used the two-compartmental neuron model (1)–(6). In the following, we treat $[K^+]_o$ in Eq. (5) as a constant parameter to determine the stable oscillatory states as a function thereof. We plot the Poincaré cross section, where the intracellular calcium level is plotted at the intersection of the membrane voltage of the axo-somatic compartment with the manifold $V = -25$ mV, for a range of $[K^+]_o \in \{4.5, 7\}$ mM. In such a plot, limit cycles are represented as points defined by a threshold crossing of a trajectory for different values of $[K^+]_o$. This method allows the graphical representation of changes in the nature of oscillatory behavior as a function of a parameter, in our case $[K^+]_o$. For a given value, tonic firing is represented as a single point, whereas bursting corresponds to a group of points. Hence, parallel lines indicate a parameter range for which bursting occurs. Here, the Poincaré cross section reveals tonic firing, coexistence of tonic firing and bursting, and only bursting for increasing levels of $[K^+]_o$ (Fig. 2). Below, we investigate the dynamics of this model neuron for different values of $[K^+]_o$ to explain the bistability between tonic firing and bursting in terms of the attractor landscape mediating the two different oscillatory states. At this point, we broadly classify the temporal activity patterns into tonic firing (which includes other nonbursting, fast activity, such as spike dou-
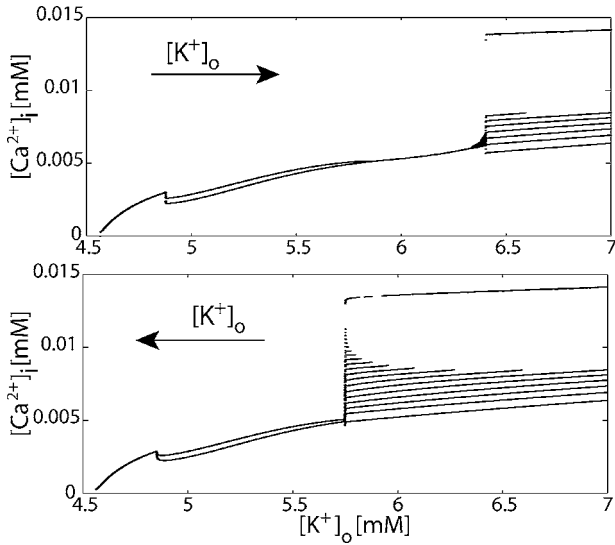
FIG. 2. Poincaré cross section for gradually increasing (top) and decreasing (bottom) $[K^+]_o$. Tonic firing corresponds to a single point, spike doublets to two points, and bursting to a series of points in the Poincaré cross section for a given value of $[K^+]_o$. Bistability between tonic firing and bursting for $[K^+]_o \in \{5.75, 6.4\}$ mM.

blets with similar frequency) and bursting, which is characterized by prolonged depolarization, quickly occasioning several spikes, before incurring in spike inactivation, followed by a pronounced after-hyperpolarization. The bifurcation analysis presented below reveals two separate dynamical mechanisms responsible for the two different activity types defined above.

To study the dynamics of bursting, we used fast-slow analysis by choosing a state variable with dynamics on the time scale of individual bursts and treating it as a parameter of the resulting reduced system. Here, the calcium-activated potassium conductance g_{KCa}, with a time scale at least as slow as the already very slow $[Ca^{2+}]_i$ dynamics, was chosen as the slow variable. As we show below, this conductance is responsible for burst termination after sufficient calcium influx via the high-threshold calcium conductance activated during the depolarized membrane state.

We first consider the case for $[K^+]_o = 5.9$ mM which is within the bistable region (see Fig. 2). Although in the full system $g_{KCa} \geq 0$ by definition, we included $g_{KCa} < 0$ in our analysis to reveal the entire bifurcation structure of the system. For all limit cycles, we show both maximum and minimum dendritic membrane voltage of the oscillatory trajectory on the ordinate of the bifurcation plots. The fixed points of the reduced system follow a z-shaped line as a function of g_{KCa} (Fig. 3, top panel). Two stable fixed points, P_s^{down} and P_s^{up}, are connected by a branch of unstable fixed points P_u. For $g_{KCa} \in \{0.007, 0.076\}$ mS/cm^2, both stable states coexist. P_s^{up} loses stability by a subcritical Andronov-Hopf bifurcation at O_1. P_s^{down} coalesces with the unstable fixed point in a saddle-node bifurcation at O_3. The following mechanism underlies burst generation in this system (Fig. 3, middle panel). Conductance g_{KCa} decreases while the system tracks P_s^{down} because of the calcium pump's efforts to remove intracellular Ca^{2+}. As a consequence, P_s^{down} eventually loses stability in
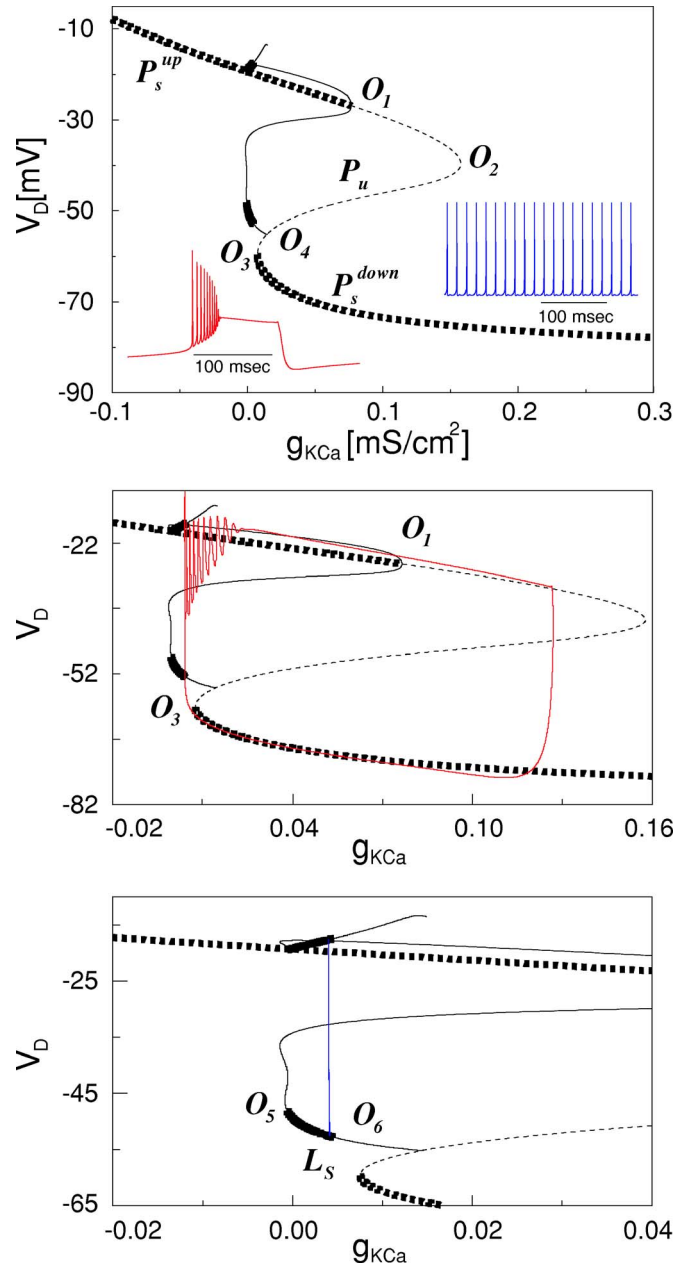
FIG. 3. (Color online) Bifurcation diagram for $[K^+]_o = 5.9$ mM. Stable fixed points P_s^{up} and P_s^{down} (thick dashed line) are connected by the branch of unstable fixed points P_u (thin dashed line). Solid lines indicate stable (thick) and unstable (thin) limit cycles. O_1, Andronov-Hopf; O_2 and O_3, fold; O_4, saddle homoclinic orbit bifurcation points. Insets show bursting and tonic spiking patterns in the complete system with freely running g_{KCa}. Middle and bottom panels, enlarged region of interest. O_5, Neimark-Sacker and O_6, period doubling bifurcation points. L_s indicates stable limit cycles. Projection of the phase trajectory for the complete system during bursting mode (solid red line, middle panel) and tonic firing (solid vertical blue line, bottom panel).

the saddle-node bifurcation point O_3 and a transition to P_s^{up} occurs. The trajectory rotates several times around P_s^{up}, which is a stable focus, but never quite reaches it in the complete system with freely running g_{KCa}. These rotations correspond to the rapid sequence of action potentials at the

onset of the burst. The decaying amplitude of the transient oscillations is reflected in the decreasing spike amplitude in the membrane voltage time-course during a burst. As the system approaches this fixed point, no more action potentials occur and the membrane voltage remains depolarized. In the meantime, the intracellular Ca^{2+} concentration increases since the cell is sufficiently depolarized to activate the high-threshold Ca^{2+} conductance which mediates calcium influx. In turn, this causes an increase in g_{KCa} which eventually leads to a loss of stability of P_s^{up} at O_1. The trajectory then falls back to P_s^{down}. In short, burst generation in the complete system is mediated by periodic transitions between two fixed points of the reduced system. These transitions form a periodic orbit corresponding to the bursting dynamics.

The small-amplitude unstable limit cycle which originates at O_1 wraps around at $g_{KCa}=-0.001$ mS/cm^2 leading to the coexistence of a small- and a large-amplitude unstable limit cycle (Fig. 3). Before coalescing with the unstable fixed point P_u in a saddle homoclinic orbit bifurcation point O_4, the unstable limit cycle with larger amplitude in the V_D dimension becomes stable in a narrow range for $g_{KCa} \in \{-0.0005, 0.0045\}$ mS/cm^2 (indicated by L_s in Fig. 3, bottom panel). At the left bifurcation point O_5, the large-amplitude cycle gains stability through a subcritical Neimark-Sacker bifurcation. At the right point O_6 the limit cycle loses stability again through a period-doubling bifurcation. Between these two points, the limit cycle L_s remains stable, mediating tonic firing. If this regime is present in the complete system with freely running g_{KCa} depends on whether g_{KCa} stays in the range where the cycle L_s is stable in the reduced system. In the complete system, g_{KCa} remains very low during tonic firing since g_{Ca} mediating calcium influx is on average only weakly activated. Also, g_{KCa} is bounded by zero on the left-hand side since an ionic conductance cannot become negative. Therefore it is critical for the existence of tonic firing in the full system that the corresponding limit cycle L_s is stable for arbitrarily small positive values of g_{KCa}. This is indeed the case for a selected value of $[K^+]_o=5.9$ mM since the left bifurcation point O_5, where the limit cycle loses stability, corresponds to a negative value of g_{KCa} and therefore permits stable tonic oscillations in the complete system. In short, the stable limit cycle of the reduced system L_s remains a stable periodic orbit in the complete system. This limit cycle mediating tonic spiking dynamics coexists with the periodic orbit mediating bursting (see above).

We next consider $[K^+]_o=5.5$ mM. In the complete system, we only observed firing with spike doublets (Fig. 2). The bifurcation diagram of the reduced system (Fig. 4) looks similar to the previous case. In contrast to $[K^+]_o=5.9$ mM, however, the limit cycle corresponding to tonic firing is unstable for $g_{KCa}>0$ mS/cm^2 (Fig. 4, right-hand inset). Instead, a cycle of period 2 is stable within a range of g_{KCa} fluctuations occurring during nonbursting activity in the complete system with freely running g_{KCa}. To determine why bursting does not occur in this system, we applied a set of perturbations of different amplitudes in the vicinity of saddle-node bifurcation point O_3 (Fig. 4). A small deflection off the saddle-node bifurcation point caused nearly periodic firing with period 4. A larger deflection left from O_3 trig-
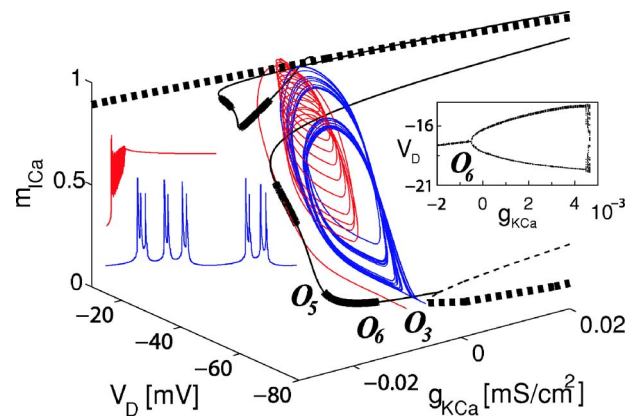
FIG. 4. (Color online) Three-dimensional bifurcation diagram for $[K^+]_o=5.5$ mM. The Z axis shows the activation variable of the high-threshold Ca^{2+} current, m_{ICa}. A small perturbation ($g_{KCa}=0.0045$ mS/cm^2) left from O_3 ($g_{KCa}=0.005$ mS/cm^2) leads to convergence to the limit cycle (blue line starting close to O_3). A larger perturbation ($g_{KCa}=0.001$ mS/cm^2) triggers convergence to the stable fixed point P_s^{up} (red line starting further away from O_3). Left-hand insets show time courses of convergence to the stable fixed point (top, red) and limit cycle (bottom, blue). Right-hand inset shows the sequence of period doubling bifurcations in Poincaré cross section, $m_{ICa}=0.4$.

gered convergence to the stable upstate fixed point P_s^{up}. Therefore, for low values of $[K^+]_o$ the vicinity of the saddle-node point O_3 no longer belongs to the basin of attraction of the upper stable fixed point P_s^{up}. For initial conditions from the low stable branch of fixed points P_s^{down}, the system reaches the saddle-node bifurcation point and then immediately jumps to the stable limit cycle with period 2, mediating firing with spike doublets.

Conversely, for $[K^+]_o=6.5$ mM (not shown), we only observed bursting in the complete system. The bifurcation plot distinguishes itself from the previous two cases by the fact that for low values of g_{KCa} there is only a very narrow region of $g_{KCa} \in \{0.01, 0.014\}$ mS/cm^2 for which a stable limit cycle L_s exists. The left bifurcation point O_5 occurs at a positive value of g_{KCa}. In the complete system, starting from the initial conditions belonging to the limit cycle, the value of g_{KCa} decreases toward its equilibrium, corresponding to a very low value of g_{KCa}. Before reaching this point, however, the limit cycle loses its stability at the Neimark-Sacker bifurcation point O_5 and the system moves to the P_s^{up} branch, starting a burst. Hence, nonbursting firing does not exist as a stable state for sufficiently elevated $[K^+]_o$.

Further elevation of $[K^+]_o$ (e.g., $[K^+]_o=9$ mM) changes the type of bifurcation point O_1 (Fig. 5). The stable up state P_s^{up} now loses stability via a supercritical Andronov-Hopf bifurcation for $g_{KCa}=0.145$ mS/cm^2 (Fig. 5, top inset). It changes the burst pattern displayed by the complete system. Rather than displaying a "smooth" transition to the low branch of fixed points P_s^{down}, the system produces a series of spikelets with increasing amplitude at the end of each depolarization state (burst offset). This particular pattern was previously described *in vivo* [13].
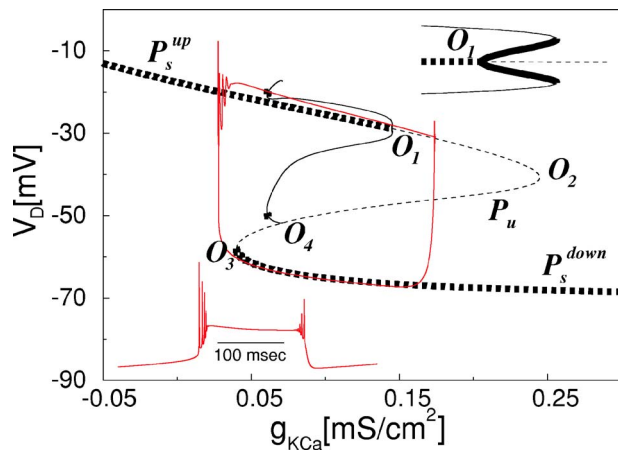
FIG. 5. (Color online) Bifurcation diagram for $[K^+]_o = 9.0$ mM. Projected trajectory of full system (thin solid line, red) shows transient oscillation at the end of the burst before switching to P_s^{down}. Top inset, supercritical Andronov-Hopf bifurcation at O_1. Bottom inset, membrane (soma, V_S) voltage time-course during burst.

IV. DISCUSSION

Extracellular potassium concentration has been shown to vary as a function of neural activity [9,10]. Specifically, potassium currents tend to increase $[K^+]_o$, whereas pumps, glial buffering, and diffusion contribute to stabilize $[K^+]_o$. When any of these mechanisms fails to operate normally, $[K^+]_o$ rises and a neuron starts to burst spontaneously [9], as frequently observed during paroxysmal seizures *in vivo* [14]. Here, we showed that nonsynaptic, spontaneous activity changes from single action potentials to bursts in conditions of increased $[K^+]_o$ in hippocampal region CA3. Our experimental approach of extracellular single unit recordings in acute hippocampal slice does not perturb the intracellular milieu (including $[Ca^{2+}]_i$, which we showed to be essential for burst termination) and is therefore free from this limitation of intracellular recordings.

Using a detailed mathematical model, we have discussed the dynamic landscape underlying the coexistence of tonic firing and bursting in a cortical pyramidal cell for elevated extracellular potassium concentration. A common mechanism of burst generation involves a transition between two attractors: a stable fixed point corresponding to a hyperpolarized state, and a limit cycle corresponding to spiking [15–17]. In our model, the fast subsystem does not have such a limit cycle attractor, and therefore spike generation depends on fast rotations around the upper fixed point with relatively weak convergence (point-point mechanisms of bursting [16]). When the trajectory approaches this stable fixed point, this corresponds to spike inactivation (depolarization block) frequently observed during seizures *in vivo* and in slices treated with high potassium and/or 4-aminopyridine (4-AP) [14].

The bursting mechanism which we described here is essentially mediated by the dynamic interaction of the high-threshold calcium conductance g_{Ca}, intracellular calcium concentration $[Ca^{2+}]_i$, and the calcium-activated potassium conductance g_{KCa}. During tonic firing, g_{Ca} is minimally activated and therefore g_{KCa} stays near its equilibrium value. This allows the spiking to continue indefinitely. In contrast, in bursting mode, substantial calcium influx mediated by g_{Ca} during the depolarized state causes g_{KCa} to activate. This in turn mediates burst termination and subsequent after-hyperpolarization. The different levels of deinactivation of g_{Ca} explain the bistability between tonic firing and bursting. In the bursting mode, g_{Ca} becomes significantly deinactivated during the hyperpolarized phase therefore enabling a rapid sequence of spikes initiating the onset of a further burst when the hyperpolarized phase is over. In contrast, when the neuron is in tonic firing mode, insufficient g_{Ca} deinactivation between spikes reduces the effect of this conductance and prevents switching to the bursting mode. The persistent sodium conductance g_{NaP} enables the existence of the bursting mode by providing additional depolarizing force to sufficiently activate g_{Ca} during the bursts. Accordingly, an increase in g_{NaP} shifts the bistable region to lower values of $[K^+]_o$. A significant decrease in g_{NaP} abolishes the bursting regime. Introducing g_h decreases the value of $[K^+]_o$ for which the neuron became active and narrowed the width of the hysteresis (data not shown).

Our model predicts the existence of a bistable regime for elevated $[K^+]_o$ where tonic firing and bursting coexist. Direct experimental verification would require a tight control of $[K^+]_o$ in the extracellular environment which is probably easier to achieve in the case of isolated neurons (e.g., in dissociated culture). Additionally, fluid dynamics of the perfusion system would need to be constrained such that $[K^+]_o$ could be rapidly increased and decreased by changing K^+ concentration at the source. Furthermore, activity-dependent changes in $[K^+]_o$ would need to be suppressed to ensure constant $[K^+]_o$.

Other potassium-mediated bistabilities between a silent and active state or between two membrane voltage values have been found both in models and experiments [18]. Bistability between tonic spiking and bursting was described in a model of a leech heart interneuron under specific pharmacological conditions [17]. Burst generation in this model was mediated by transitions between a fixed point and a periodic orbit of the fast subsystem and included bursting regimes with arbitrary long oscillatory depolarized states.

Existence of bistability between tonic spiking and bursting for an intermediate range of $[K^+]_o$ predicts that in a neuronal system with dynamically updated $[K^+]_o$, K^+-dependent regulation of neuronal activity may lead to complex oscillatory behavior [19]. In an isolated neuron model where $[K^+]_o$ was continuously computed based on neuronal K^+ currents, K^+ pumps and glial buffering, $[K^+]_o$ decreased faster during periodic bursting and slower during tonic firing [9]. Since the $[K^+]_o$ gradient depends on the frequency of firing, excitation mediated by lateral synaptic connections between neurons may increase the frequency of tonic spiking sufficiently to provide $[K^+]_o$ elevation during tonic spiking throughout the network of neurons. On the other hand, frequency of bursting is mainly mediated by intrinsic cell properties—rate of deactivation of the calcium-dependent potassium conductance

during the intraburst interval—and, therefore, the $[K^+]_o$ gradient during bursting can stay negative even in the presence of excitatory synaptic connections. This suggests that activity-dependent modulation of intrinsic excitability can lead to sustained oscillations in a cortical network with slow transitions between two distinct firing modes—tonic spiking and bursting—mediated by slow $[K^+]_o$ oscillations. Examples from *in vivo* experiments where such transitions were observed include the transition between fast runs and slow bursting during spike-wave seizures [20] and periodic transitions between slow-wave and fast-wave oscillations in olfactory cortex [21].

[1] C. M. Gray, P. Konig, A. K. Engel, and W. Singer, Nature (London) **338**, 334 (1989); T. Womelsdorf, P. Fries, P. P. Mitra, and R. Desimone, *ibid.* **439**, 733 (2006); R. Stickgold, L. James, and J. A. Hobson, Nat. Neurosci. **3**, 1237 (2000); P. Maquet, Science **294**, 1048 (2001).

[2] M. Steriade, D. A. McCormick, and T. J. Sejnowski, Science **262**, 679 (1993); M. Steriade, I. Timofeev, and F. Grenier, J. Neurophysiol. **85**, 1969 (2001); S. M. Sherman, Trends Neurosci. **24**, 122 (2001); G. G. Turrigiano, E. Marder, and L. F. Abbott, J. Neurophysiol. **75**, 963 (1996); A. Shilnikov and G. Cymbalyuk, Phys. Rev. Lett. **94**, 048101 (2005).

[3] M. S. Jensen and Y. Yaari, J. Neurophysiol. **77**, 1224 (1997); A. Leschinger, J. Stabel, P. Igelmund, and U. Heinemann, Exp. Brain Res. **96**, 230 (1993); E. Pan and J. L. Stringer, J. Neurophysiol. **77**, 2293 (1997).

[4] W. J. Moody, K. J. Futamachi, and D. A. Prince, Exp. Neurol. **42**, 248 (1974); I. Dietzel, U. Heinemann, and H. D. Lux, Glia **2**, 25 (1989); G. G. Somjen, *Ions in the Brain: Normal Function, Seizures, and Stroke* (Oxford University Press, New York, 2004).

[5] S. F. Traynelis and R. Dingledine, J. Neurophysiol. **59**, 259 (1988).

[6] Z. F. Mainen and T. J. Sejnowski, Nature (London) **382**, 363 (1996).

[7] The $I_{Na,D}$ current has $M=3$, $H=1$, $A_m=0.182(V_D+25)/\{1-\exp[-(V_D+25)/9]\}$, $B_m=0.124(-V_D-25)/\{1-\exp[-(-V_D-25)/9]\}$, $A_h=0.024(V_D+40)/\{1-\exp[-(V_D+40)/5]\}$, $B_h=0.0091(-V_D-65)/\{1-\exp[-(-V_D-65)/5]\}$, $\tau_m=1/[\alpha(A_m+B_m)]$, $\tau_h=1/[\alpha(A_h+B_h)]$, $m_\infty=A_m/(A_m+B_m)$, $h_\infty=1/\{1+\exp[(V_D+55)/6.2]\}$. The $I_{Nap,D}$ current has $M=1$, $H=0$, $m_\infty=0.02/\{1+\exp[-(V_D+42)/5]\}$, $\tau_m=0.1992$. The I_{Km} current has $M=1$, $H=0$, $A_m=0.001(V_D+30)/\{1-\exp[-(V_D+30)/9]\}$, $B_m=-0.001(V_D+30)/\{1-\exp[(V_D+30)/9]\}$, $\tau_m=1/[\alpha(A_m+B_m)]$, $m_\infty=A_m/(A_m+B_m)$. The I_{KCa} current has $M=2$, $H=0$, $m_\infty=(48[Ca^{2+}]_i^2/0.03)/(48[Ca^{2+}]_i^2/0.03+1)$, $\tau_m=\{1/[0.03(48[Ca^{2+}]_i/0.03+1)]\}/4.6555$. The I_{Ca} current has $M=2$, $H=1$, $A_m=0.055(-27-V_D)/\{\exp[(-27-V_D)/3.8]-1\}$, $B_m=0.94\exp[(-75-V_D)/17]$, $\tau_m=1/[\alpha(A_m+B_m)]$, $m_\infty=A_m/(A_m+B_m)$, $A_h=0.000\,457\exp[(-13-V_D)/50]$, $B_h=0.0065/\{\exp[(-V_D-15)/28]+1\}$, $\tau_h=1/[\alpha(A_h+B_h)]$, $h_\infty=A_h/(A_h+B_h)$. The I_h current has $M=1$, $H=0$, $m_\infty=1/\{1+\exp[(V_D+82)/7]\}$, $\tau_m=38$.

[8] The sodium currents are of identical form as for the dendritic compartment except for the maximal conductances (see main text). The current I_{Kv} has $M=4$, $H=0$, $A_m=0.02(V_S-25)/\{1-\exp[-(V_S-25)/9]\}$, $B_m=-0.002(V_S-25)/\{1-\exp[(V_S-25)/9]\}$, $\tau_m=1/[\alpha(A_m+B_m)]$, $m_\infty=A_m/(A_m+B_m)$.

[9] M. Bazhenov, I. Timofeev, M. Steriade, and T. J. Sejnowski, J. Neurophysiol. **92**, 1116 (2004).

[10] H. Kager, W. J. Wadman, and G. G. Somjen, J. Neurophysiol. **84**, 495 (2000).

[11] XPP-Aut: X-Windows PhasePlane plus AUTO, G. Bard Ermentrout, Department of Mathematics, University of Pittsburgh, Pittsburgh, USA. http://www.pitt.edu/~phase

[12] Transverse hippocampal slices (400 μm) from a male Wistar rat (p18) were cut in ice cold standard artificial cerebrospinal fluid (ACSF) equilibrated with 95% O_2 and 5% CO_2 (119 mM NaCl, 2.5 mM KCl, 1.3 mM NaHPO$_4$, 1.3 mM MgCl$_2$, 2.5 mM CaCl$_2$, 26 mM NaHCO$_3$, and 11 mM glucose) and then transferred into an interface chamber where they were incubated at 34 °C for 45 minutes. A multiwire electrode (ALA Scientific, Westbury, NY) was used for recording spontaneous spiking activity in CA3. Fast synaptic transmission was blocked by bath application of 10 μM NBQX and 2.5 μM Gabazine (Tocris Bioscience, Ellisville, MO). Slices were submerged in standard ACSF (32 °C); the high potassium condition corresponded to an increase of KCl concentration to 6.5 mM. Extracellular traces were band pass filtered (300 Hz, 5000 kHz) and sampled at 20 kHz. Potential spikes were detected by threshold crossing. A spike from a given unit was typically picked up by 3–4 recording sites (tetrodelike recordings). Spikes were then sorted by first overclustering the wave forms into subclusters with the k-means clustering algorithm. As a result, spikes corresponding to a single unit were represented by several neighboring subclusters. These subclusters were then manually combined to clusters representing individual units. Details in M. S. Fee, P. P. Mitra, and D. Kleinfeld, J. Neurosci. Methods **69**, 175 (1996). All experiments were carried out in accordance with the guidelines set forth by the University of California.

[13] M. Steriade, F. Amzica, D. Neckelmann, and I. Timofeev, J. Neurophysiol. **80**, 1456 (1998).

[14] M. Steriade and D. Contreras, J. Neurosci. **15**, 623 (1995); P. Perreault and M. Avoli, J. Neurophysiol. **61**, 953 (1989); J. Ziburkus, J. R. Cressman, E. Barreto, and S. J. Schiff, *ibid.* **95**, 3948 (2006).

[15] J. Rinzel and B. Ermentrout, in *Methods in Neural Modeling*, edited by C. Koch and I. Segev (MIT Press, Cambridge, Massachusetts, 1998).

[16] E. M. Izhikevich, Int. J. Bifurcation Chaos Appl. Sci. Eng. **10**,

1171 (2000).

[17] A. Shilnikov, R. L. Calabrese, and G. Cymbalyuk, Phys. Rev. E **71**, 056214 (2005).

[18] P. J. Hahn and D. M. Durand, J. Comput. Neurosci. **11**, 5 (2001); D. C. Gadsby and P. F. Cranefield, J. Gen. Physiol. **70**, 725 (1977); G. L. Yuen, P. E. Hockberger, and J. C. Houk, Biol. Cybern. **73**, 375 (1995); J. R. McCullough, W. T. Chua, H. H. Rasmussen, R. E. Ten Eick, and D. H. Singer, Circ. Res.

66, 191 (1990).

[19] F. Fröhlich, M. Bazhenov, I. Timofeev, M. Steriade, and T. J. Sejnowski, J. Neurosci. **26**, 6153 (2006).

[20] I. Timofeev, F. Grenier, and M. Steriade, J. Neurophysiol. **80**, 1495 (1998).

[21] M. Murakami, H. Kashiwadani, Y. Kirino, and K. Mori, Neuron **46**, 285 (2005).